

Reservoir description using a binary level set model

Lars Kristian Nielsen · Hongwei Li · Xue-Cheng Tai ·
Sigurd Ivar Aanonsen · Magne Espedal

Received: 7 September 2005 / Accepted: 23 May 2008
© Springer-Verlag 2008

Abstract We consider the inverse problem of permeability estimation for two-phase flow in porous media. In the parameter estimation process we utilize both data from the wells (production data) and spatially distributed data (from time-lapse seismic data). The problem is solved by approximating the permeability field by a piecewise constant function, where we allow the discontinuity curves to have arbitrary shape with some forced regularity. To achieve this, we have

utilized level set functions to represent the permeability field and applied an additional total variation regularization. The optimization problem is solved by a variational augmented Lagrangian approach. A binary level set formulation is used to determine both the curves of discontinuities and the constant values for each region. We do not need any initial guess for the geometries of the discontinuities, only a reasonable guess of the constant levels is required.

Communicated by G. Wittum.

L. K. Nielsen · X.-C. Tai · S. I. Aanonsen · M. Espedal
Department of Mathematics,
University of Bergen, 5020 Bergen, Norway
e-mail: tai@math.uib.no

M. Espedal
e-mail: resme@math.uib.no

L. K. Nielsen · H. Li · S. I. Aanonsen (✉) · M. Espedal
CIPR-Centre for Integrated Petroleum Research,
University of Bergen, 5020 Bergen, Norway
e-mail: Sigurd.Aanonsen@cipr.uib.no

H. Li
Department of Mathematics, Capital Normal University,
10037 Beijing, People's Republic of China
e-mail: lihw@mail.cnu.edu.cn

X.-C. Tai
Division of Mathematical Sciences,
School of Physical and Mathematical Sciences,
Nanyang Technological University,
Singapore 637616, Singapore
e-mail: xctai@ntu.edu.sg

Present address:

L. K. Nielsen
Laksevåg Upper Secondary/High School,
Bergen, Norway
e-mail: larnie@hfk.no

Keywords Inverse problems · Reservoir description · Parameter identification · Two-phase flow · Level set methods · Augmented Lagrangian optimization · Total variation regularization

1 Introduction

Predictions of the reservoir behaviour require estimates of the reservoir property values, such as permeability and porosity, on a grid block scale. Even if all available data sources are utilized, this can be a very difficult task. Large scale permeability trends, like barriers and channels, have large impact on how the fluids flow in the porous medium. Information of these structures is therefore important for the reservoir engineers controlling the production in the reservoir.

Available data types for estimating permeability and porosity inside a reservoir are geological data, seismic data and static and dynamic well data. The geological data are usually coarsened geological permeability maps, and the seismic data are several seismic surveys taken at different times through the production history. The seismic data contains information of fluid movement and pressure changes. The static well data can be obtained from core samples in the wells, while the dynamic well data are time series of pressures and flow rates in the wells.

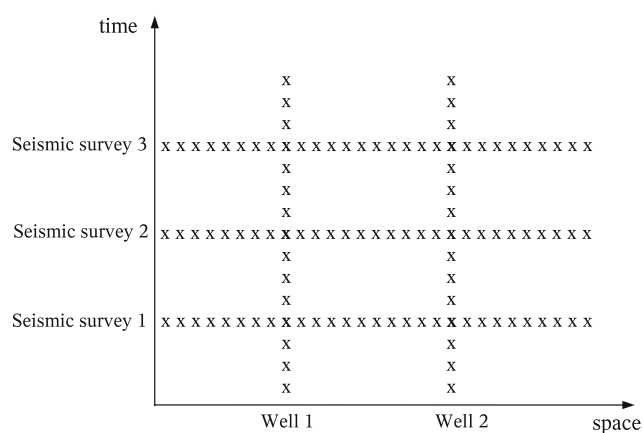


Fig. 1 Distribution of measurements in time and space. The well data is sparsely distributed in space, while the time frequency is high. The seismic data have the opposite characterization, with high frequency in space but a lower frequency in time. The two data sources give complementary information in the time and space domain, but the total amount of data is still sparse because of the low frequency directions

Neither the seismic data nor the dynamic well data give any direct information of the permeability and porosity fields. Using the equations of fluid flow, we can though use the indirect information from these measurements to estimate the permeability and the porosity on a coarse scale. A problem of this kind is generally known as an inverse problem, or more specific referred to as a *history matching* problem. In this paper, we focus on the problem of recovering the permeability trends by utilizing the information from the wells (both static and dynamic) together with the seismic data.

Because of the high costs of drilling a well, the well data is available from only a very small part of the reservoir, but the time frequency of this data can be high. Contrary to the well data, the seismic surveys can also give information in the regions between and beyond the wells. The seismic data will in this way give information from larger parts of the spatial domain, but the frequency in time will be low. By utilizing both well data and seismic data, we have complementary information in the time and space domain. However, the total amount of data may still be sparse, see Fig. 1.

The incorporation of 4D seismic data (time-lapse data) is relatively new in history matching. A quantitatively incorporation of these data has been discussed by Gosselin et al. [16]. Aanonsen et al. [1, 2] have taken this approach further and considered the effect of using proper weights for the seismic data in the objective function.

It is well known that inverse problems are often ill-conditioned. The sparse distribution of the data will usually make the conditioning of the inverse problem worse [10]. To get a meaningful solution, we have to regularize the problem in a proper way. This can be done by restricting the parameter space in order to exclude non-physical solutions.

A number of methods has been applied to regularize similar inverse problems as described above. One strategy is to penalize deviations from a priori knowledge of the solution. This knowledge can be given by a geological model. An example of this approach is Bayesian estimation, see, e.g. [13, 30]. Another strategy is to force the solution to be piecewise constant. One way to achieve this is to use a zonation, that is, dividing the domain into clusters of grid blocks, where each cluster has constant permeability. The zonation can be chosen a priori or it can be determined gradually through a sequence of parameter estimation problems, see, e.g. [17]. In these approaches there are usually strong restrictions on the shape of the clusters of grid blocks with different constant permeability values. In [6, 22] these restrictions have been loosened by combining a multiscale zonation strategy with a level set approach.

Contrary to the referred approaches, which utilize only well data, we have also incorporated seismic measurements in the observation data in this work. As described before, the total amount of data may then be higher, and we may therefore be able to find solutions on slightly finer scales than what is searched for with only well data present.

Based on the assumption of more available information, we will in this paper propose a method that the estimation of the permeability is done directly by a level set approach, that is, without any coarse scale parameterization method to predict an initial guess as used in [6, 22]. By the level set formulation, we restrict the estimate to be piecewise constant. The geometries of the discontinuity curves are allowed to be arbitrary, but with some forced regularity achieved by a total variation regularization.

Level set methods can produce piecewise constant solutions with a predefined number of constant levels. If the sought solution has fewer regions than this predefined number, the estimate will leave one or more regions empty. In this way, we only need an upper bound for the number of regions in the piecewise constant solution.

The original level set method was proposed by Osher and Sethian [25] for tracing interfaces between different phases of fluid flow. It has later been a versatile tool for representing and tracking interfaces separating a domain into subdomains. The method has been applied in a wide range of applications, i.e. inverse problems, image analysis and optimal shape design problems. For a recently survey of level set methods, see [28]. Examples of level set methods applied to inverse problems can be found in [3–5, 7–9, 11, 12, 18, 26].

In this work, we will apply a variant of a *piecewise constant level set method* [20, 21, 24, 29]. In these methods, the level set functions are discontinuous and have discontinuities at the boundaries of the subdomains. The method of choice is a *binary level set method*, where the level set functions are required to take only the values 1 and -1 at convergence. This method has previously been applied to segmentation

of digital images [21] and solving inverse elliptic problems [24]. Here we will apply the same framework for solving the history matching problem.

A requirement for applying the level set method to this problem is that we have indications of a piecewise constant field. In geological terms, this means that the reservoir contains different *facies*, where the properties are approximately constant within each facies, but the exact geometry is unknown. Normally, suitable bounds for the number of facies and the constant levels within each facies will be available. The method presented in the paper is a multiple level set approach which is able to find an arbitrary number of regions. In the numerical part, we will though restrict ourselves to look at fields that have indications of a channelled system with two different levels (facies).

The paper is organized in the following way: in Sect. 2 the model equations are given, and in Sect. 3 the inverse problem is defined. The general framework for the binary level set approach is presented in Sect. 4, while we in Sect. 5 explain how this framework is utilized to solve the inverse problem. Further the numerical optimization method and the applied algorithm are given in Sect. 6. Some implementation issues are discussed in Sect. 7, and the numerical results are presented in Sect. 8. Finally the conclusions are given in Sect. 9.

2 Model equations

Assuming only oil and water presented in a porous medium with isotropic permeability, the conservation equations for two-phase incompressible, immiscible, horizontal flow are

$$\Phi(\mathbf{x}) \frac{\partial S_o}{\partial t} - \nabla \cdot \left(\frac{\kappa(\mathbf{x}) \kappa_{ro}(S_o)}{\mu_o} \nabla p_o \right) = f_o(\mathbf{x}), \quad (1)$$

$$\Phi(\mathbf{x}) \frac{\partial S_w}{\partial t} - \nabla \cdot \left(\frac{\kappa(\mathbf{x}) \kappa_{rw}(S_w)}{\mu_w} \nabla p_w \right) = f_w(\mathbf{x}), \quad (2)$$

where $(\mathbf{x}, t) \in \Omega \times [0, T]$. $\Omega \in \mathbb{R}^2$ is a bounded reservoir domain and the subscripts o and w refer to the phases, water and oil, respectively. S_i denotes the saturation, μ_i the viscosity, p_i the pressure, f_i the external volumetric flow rate and κ_{ri} is the relative permeability, where i is the fluid phase. The porosity and the absolute permeability are given by $\Phi(\mathbf{x})$ and $\kappa(\mathbf{x})$, respectively.

In addition, we assume a completely saturated medium,

$$S_o + S_w = 1, \quad (3)$$

and suppose we have a function P_c defining the capillary pressure,

$$p_o - p_w = P_c. \quad (4)$$

The quantities Φ , κ , κ_{ri} and P_c are all dependent of the porous medium and are not accessible through direct measurements.

The problem treated in this paper is to find an estimate of the absolute permeability, $\kappa(\mathbf{x})$, while Φ and κ_{ri} are assumed to be known, and P_c is set to zero. Equations (1)–(4) define this task as an inverse problem.

3 The inverse problem

Because of the nature of the permeability, it is more natural to solve the optimization problem with respect to the logarithm of the permeability instead of the permeability itself. For notational matter, we define

$$q(\mathbf{x}) = \log_{10} \kappa(\mathbf{x}), \quad (5)$$

and solve the problem with respect to $q(\mathbf{x})$. The transformation from κ till q will only influence the jumps between the different permeability zones, and not the contour of the discontinuities. This is because a piecewise constant κ is equivalent to a piecewise constant q . When obtaining a solution, the estimate of $q(\mathbf{x})$ can easily be transformed back to the permeability $\kappa(\mathbf{x})$ through Eq. (5).

Let \mathbf{d}_{well} be a vector of well data, and \mathbf{d}_{seis} be a vector of seismic data, and assume that all measurements have been transformed into pressures and saturations:

$$\mathbf{d}_{\text{well}} = \{p_o(\mathbf{x}_{\text{well},i}, t), S_w(\mathbf{x}_{\text{well},i}, t) \text{ for } i = 1, 2, \dots, n_{\text{well}}, t \in [0, T]\}, \quad (6)$$

$$\mathbf{d}_{\text{seis}} = \{p_o(\mathbf{x}, t_j), S_w(\mathbf{x}, t_j) \text{ for } \mathbf{x} \in \Omega, j = 1, 2, \dots, n_{\text{seis}}\}, \quad (7)$$

where n_{well} is the number of present wells in Ω and n_{seis} is the number of seismic surveys in the time domain $[0, T]$.

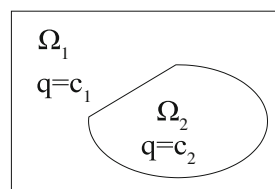
When incorporating different kinds of data in one optimization process, it is important to weight the different data types properly. As in [1, 2] we apply the following objective function to measure the misfit between the measured and the simulated data

$$\begin{aligned} J_{\text{tot}}(q) &= J_{\text{well}}(q) + J_{\text{seis}}(q) \\ &= \frac{1}{2} (\mathbf{d}_{\text{well}} - \mathbf{m}_{\text{well}}(q))^T D_{\text{well}}^{-1} (\mathbf{d}_{\text{well}} - \mathbf{m}_{\text{well}}(q)) \\ &\quad + \frac{1}{2} (\mathbf{d}_{\text{seis}} - \mathbf{m}_{\text{seis}}(q))^T D_{\text{seis}}^{-1} (\mathbf{d}_{\text{seis}} - \mathbf{m}_{\text{seis}}(q)). \end{aligned} \quad (8)$$

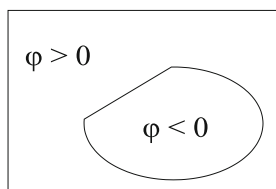
Here $\mathbf{m}_{\text{well}}(q)$ and $\mathbf{m}_{\text{seis}}(q)$ are the simulated values corresponding to the given measurements. These values are calculated by the forward model [Eqs. (1)–(4)] for a given function $q(\mathbf{x})$ [or corresponding permeability function $\kappa(\mathbf{x})$]. D_{well} and D_{seis} are the covariance matrices representing the data error.

Fig. 2 Level set representations of a piecewise constant function $q(\mathbf{x})$. In this example q has two regions with different constant values, c_1 and c_2 .

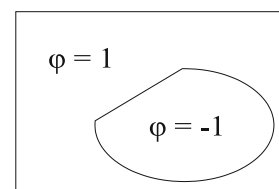
By continuous level set functions the discontinuity of q can be represented as in **b**, and by binary level set functions ϕ is forced to take the values -1 and 1 , as in **c**



(a) The discontinuity of a piecewise constant function $q(\mathbf{x})$.



(b) Continuous level set func.



(c) Binary level set func.

The problem of recovering $q(\mathbf{x})$ is an inverse problem which can be highly ill-posed. Because of the ill-posedness, a proper regularization is required to restrict the solution space. In this work, we restrict the solution to be piecewise constant. We will allow arbitrary shapes of the geometries of the discontinuity curves, but with some restrictions related to the regularity of q . As in [9,24] this is achieved by applying a total variation based regularization together with the piecewise constant requirement. The actual applied regularization is

$$R(q) = \int_{\Omega} |\nabla q| \, d\mathbf{x}, \tag{9}$$

and this will control both the length of the interfaces and the jumps of q .

The functional to be minimized is defined as

$$F(q) = J_{\text{tot}}(q) + \beta R(q), \tag{10}$$

where $\beta > 0$ is a parameter weighting the amount of regularization. The inverse problem is solved by finding the optimal function q^* , which is the solution of the following minimization problem:

$$q^* = \arg \min_{q \in Q} F(q), \tag{11}$$

where Q is the space of piecewise constant functions.

4 The binary level set approach

In this section, we will present the binary level set formulation. The general framework for this method was first proposed in [21] where it was applied to segmentation of digital images. Some of the essential ideas for this method have appeared earlier in [15,27]. The binary level set method has later been used in [24] for solving inverse elliptic problems. In the present work, we will follow the approach in [24]

and utilize the level set functions to construct a piecewise constant coefficient function as a solution to an inverse problem. The actual inverse problem is here defined in Sect. 3.

In standard level set methods, continuous level set functions are used to partition a domain Ω into a number of subdomains $\{\Omega_j\}$. The boundaries (or interfaces) between the subdomains are defined by the sign changes of the level set functions, and for numerical reasons the level set functions are forced to be (close to) signed distance functions. In the binary formulation, we will instead use discontinuous level set functions which at convergence should take the values -1 or 1 , inside and outside the subdomains. The discontinuities of the functions will represent the boundary of the subdomains.

Let us first assume that Ω needs to be divided into two subdomains, Ω_1 and Ω_2 , such that $\Omega_1 \cap \Omega_2 = \emptyset$ and $\Omega = \bar{\Omega}_1 \cup \bar{\Omega}_2$, where $\bar{\Omega}_j$ is the closure of Ω_j . A representation of this domain can be given by

$$\phi(\mathbf{x}) = \begin{cases} 1 & \forall \mathbf{x} \in \Omega_1 \\ -1 & \forall \mathbf{x} \in \Omega_2, \end{cases} \tag{12}$$

and the curve separating Ω_1 and Ω_2 is implicitly given as the discontinuity of ϕ , see Fig. 2. The properties of ϕ can be used to construct a scalar function $q(\mathbf{x})$ with distinct constant values inside the two different subdomains. If we assume that the value of $q(\mathbf{x})$ is equal to c_1 in Ω_1 and equal to c_2 in Ω_2 , then q can be written as

$$q = \frac{1}{2} [c_1(\phi + 1) - c_2(\phi - 1)]. \tag{13}$$

As in the continuous level set formulation, multiple level set functions can be used to represent more than two regions. Following the terminology applied in [21], a function having four constant regions can be represented by two level set

functions, and expressed as

$$q = \frac{1}{4} [c_1(\phi_1 + 1)(\phi_2 + 1) - c_2(\phi_1 + 1)(\phi_2 - 1) - c_3(\phi_1 - 1)(\phi_2 + 1) + c_4(\phi_1 - 1)(\phi_2 - 1)]. \quad (14)$$

Further, N binary level set functions can be combined to produce a function with 2^N different levels. Given $\boldsymbol{\phi} = \{\phi_i\}_{i=1}^N$ and $\mathbf{c} = (c_1, c_2, \dots, c_{2^N})$, the function q can be expressed as the sum

$$q(\boldsymbol{\phi}, \mathbf{c}) = \sum_{j=1}^{2^N} c_j \psi_j(\boldsymbol{\phi}). \quad (15)$$

where ψ_j are basis functions which are dependent on $\boldsymbol{\phi}$. An expression for ψ_j is omitted here, but can be found in [24]. Equations (13) and (14) are special cases of Eq. (15). In the first case, we have $\psi_1 = \frac{1}{2}(\phi + 1)$ and $\psi_2 = -\frac{1}{2}(\phi - 1)$ in Eq. (13). With two level set functions, we get $\psi_1 = \frac{1}{4}(\phi_1 + 1)(\phi_2 + 1)$, $\psi_2 = -\frac{1}{4}(\phi_1 + 1)(\phi_2 - 1)$, \dots in Eq. (14).

In the following, we let $K(x) = x^2 - 1$. The level set functions are required to satisfy the constraint

$$K(\phi_i) = \phi_i^2 - 1 = 0 \quad \forall i. \quad (16)$$

This requirement will force the level set functions to take the values -1 or 1 at convergence. With (16) fulfilled, the basis functions will be characteristic functions for the corresponding subdomains, i.e. $\psi_j = 1$ in Ω_j and zero elsewhere. That is, the support of the different basis functions are non-overlapping, $\text{supp } \psi_i \cap \text{supp } \psi_j = \emptyset \quad \forall i \neq j$, and the total support of all the basis functions covers the complete domain, i.e. $\Omega = \cup_{j=1}^{2^N} \text{supp } \psi_j$.

5 The binary level set method for the inverse problem

From the last section, we see that every piecewise constant function can be represented as in (15) under the requirement that the level set functions satisfy (16). In order to find a piecewise constant function, we just need to find the corresponding c_j values and the level set functions ϕ_i . If we define the vector $\mathbf{K}(\boldsymbol{\phi}) = \{K(\phi_i)\}_{i=1}^N$, we can thus reformulate problem (11) as

$$(\boldsymbol{\phi}^*, \mathbf{c}^*) = \arg \{ \min_{\boldsymbol{\phi}, \mathbf{c}} F(q(\boldsymbol{\phi}, \mathbf{c})) \text{ subject to } \mathbf{K}(\boldsymbol{\phi}) = \mathbf{0} \}, \quad (17)$$

where the optimal coefficient can be calculated by $q^* = q(\boldsymbol{\phi}^*, \mathbf{c}^*)$. The constraint $\mathbf{K} = \mathbf{0}$ is applied to control the structure of the level set functions, and will therefore depend on the choice of basis functions.

Define $\tilde{F}(\boldsymbol{\phi}, \mathbf{c}) = F(q(\boldsymbol{\phi}, \mathbf{c}))$. To evolve the level set functions and update the constant values such that $q(\mathbf{x})$ will converge to the optimal solution, we need to calculate the

derivatives of \tilde{F} with respect to $\boldsymbol{\phi}$ and \mathbf{c} . By the chain rule we have, cf. [9],

$$\frac{\partial \tilde{F}}{\partial \phi_i} = \frac{\partial F}{\partial q} \frac{\partial q}{\partial \phi_i} \quad \forall i = 1, 2, \dots, N \quad (18)$$

and

$$\frac{\partial \tilde{F}}{\partial c_j} = \int_{\Omega} \frac{\partial F}{\partial q} \frac{\partial q}{\partial c_j} d\mathbf{x} \quad \forall j = 1, 2, \dots, 2^N. \quad (19)$$

The time consuming part of these calculations is to find $\frac{\partial F}{\partial q}$. In this work $\frac{\partial F}{\partial q}$ is calculated by adjoint gradient calculations (see, e.g. [19]) in a reservoir simulator.

It could be mentioned that the method presented here has some similarities with more “traditional” methods based on the assumption that the permeability can be represented by truncated Gaussian or pluri-Gaussian random fields, like the method presented by Liu and Oliver [23]. In both cases the update is based on the gradient $\partial F / \partial q$ (Eq. 19), obtained from the adjoint equations. However, in our approach, the Gaussian fields to be estimated are replaced by the level set functions. In the truncated Gaussian method, a regularization term based on a prior Gaussian distribution is used, while we use a total variation regularization to control the lengths of the interfaces and the jumps. In [23], the shapes of three different geological facies were estimated using two Gaussian fields (corresponding to two level set functions). However, a truncation rule, defining the transition between the facies, as well as the constant values of the properties within each region, were assumed known. With respect to efficiency of our method, the number of iterations required to match the data is comparable to the traditional method, while it takes many iterations to fulfill the constraint $\mathbf{K}(\boldsymbol{\phi}) = \mathbf{0}$, which ensures that the solution is piecewise constant at convergence.

6 Numerical optimization

We apply an augmented Lagrangian method to solve problem (17) numerically. The Lagrangian functional involves both \tilde{F} and the constraint K ;

$$L(\boldsymbol{\phi}, \mathbf{c}, \boldsymbol{\lambda}) = \tilde{F}(\boldsymbol{\phi}, \mathbf{c}) + \sum_{i=1}^N \int_{\Omega} \lambda_i K(\phi_i) dx + \mu_p \sum_{i=1}^N \int_{\Omega} |K(\phi_i)|^2 dx. \quad (20)$$

Here $\mu_p > 0$ is a penalization parameter which usually is a fixed parameter chosen a priori, or it can in some cases be increased carefully through the iterations to improve the convergence. $\boldsymbol{\lambda} = \{\lambda_i\}_{i=1}^N$ is the Lagrangian multipliers where λ_i is a function defined in the same domain as ϕ_i .

We search a saddle point of L and therefore require

$$\begin{aligned} \frac{\partial L}{\partial \phi_i} = 0, \quad \frac{\partial L}{\partial \lambda_i} = 0 \quad \forall i \in \{1, \dots, N\} \\ \text{and} \quad \frac{\partial L}{\partial c_j} = 0 \quad \forall j \in \{1, \dots, 2^N\}. \end{aligned} \quad (21)$$

Starting with initial guesses ϕ^0 , \mathbf{c}^0 and λ^0 , we iterate towards the better approximations denoted by ϕ^k , \mathbf{c}^k and λ^k where $k = \{1, 2, \dots\}$. These variables are updated using a steepest descent method, and when the change of the variables approaches zero, the iterations can be stopped. Expressions of the gradients in (21) and a more detailed description of the numerical updates can be found in [24]. In [29] a MBO operator splitting scheme has been applied for solving related problems.

Because of the computationally effort to run the forward model, we have in this work applied a fixed timestep when updating ϕ instead of the line search applied in [24]. The updating of each c_j is less stable than the updating of ϕ , so to update \mathbf{c} , we have used separate line searches for each c_j to prevent choosing timesteps that will increase the value of \tilde{F} . The actual applied algorithm is as follows:

Algorithm A (Uzawas algorithm for variational level set methods)

Determine how many level set functions, N , to use.

Choose timestep for ϕ : Δt_ϕ .

Choose search interval for each c_j : $c_j \in [a_j, b_j]$.

Initialize: ϕ^0 , \mathbf{c}^0 and λ^0 and set $k = 0$.

1. Update ϕ ;

- (a) Compute q by Eq. (15).
- (b) Evolve the level set functions:

$$\phi^{k+1} = \phi^k - \Delta t_\phi \frac{\partial L}{\partial \phi}(\phi^k, \mathbf{c}^k, \lambda^k).$$

2. Update \mathbf{c} (after a fixed number of iterations);

For each c_j , $j = 1, 2, \dots, 2^N$:

- (a) Compute q by Eq. (15).
- (b) Define: $\alpha_{c_j}^k = \frac{\partial L}{\partial c_j}(\phi^{k+1}, \mathbf{c}^k, \lambda^k)$.
- (c) Define the search interval: Let $M \in \mathbb{R}$ be all values of Δt such that $c_j^k - \Delta t \alpha_{c_j}^k \in [a_j, b_j]$.
- (d) Find the optimal timestep: $\Delta t_{c_j} = \arg \min_{\Delta t \in M} L(\phi^{k+1}, \mathbf{c}^k - \Delta t \alpha_{c_j}^k \mathbf{e}_j, \lambda^k)$, where \mathbf{e}_j is the j 'th unit vector.
- (e) Update this constant: $c_j^{k+1} = c_j^k - \Delta t_{c_j} \alpha_{c_j}^k$.

3. Update λ (after a fixed number of iterations);

$$\lambda^k = \lambda^k + \mu \mathbf{K}(\phi^{k+1}).$$

4. Iterate again if necessary;

$$k = k + 1.$$

Notice that q is updated implicitly using the most recently calculated values of ϕ and \mathbf{c} . In this algorithm we do not use step 2 and 3 in every iteration. This is because the algorithm becomes unstable if \mathbf{c} and λ are updated too often. In principle we could have run step 1 to convergence before doing the other steps. Numerically this is not strictly necessary and it would have been computationally heavy. We have therefore updated \mathbf{c} and λ after a fixed number of iterations.

7 Implementation issues

7.1 Discretization

For all the numerical experiments, the reservoir dimension is $1,000 \text{ m} \times 1,000 \text{ m} \times 40 \text{ m}$. This domain is decomposed into $16 \times 16 \times 1$ cells. The actual computational grid consists of all the cell centers. For our in-house forward simulator, we use the control-volume method to discretize 1 and 2. The permeability field as well as the level set functions are discretized on the same $16 \times 16 \times 1$ grid.

It's worth to point out that, during the iterations of **Algorithm A**, the level set functions are changing continuously to approximate some piecewise constant functions, and they are not piecewise constant during the iterations, even with the special acceleration technique described below. In this sense, the interface represented by the level set functions is missing during the iterations. However, for our method, the exact location of the interface is not so important during the iterations. After convergence, the level set functions should be piecewise constant, or well behaved as piecewise constant.

7.2 Acceleration techniques

As is typical for Augmented Lagrangian algorithms, the convergence is fast in the beginning and it slows down when the solution is getting closer to the true minimizer. A natural remedy to this, is to apply larger timesteps when evolving ϕ , but this will make the algorithm unstable. Another problem, when solving inverse problems, is that the sensitivities related to changes in the data with respect to q may be very small in some regions. This will further slow down the speed of convergence.

As in [24] we have used a modification of the original binary level set function to speed up the convergence of the method. When computing $q = q(\phi, \mathbf{c})$ we have replaced

each ϕ_i by the function

$$\tilde{\phi}_i = \text{sgn}(\phi_i) = \begin{cases} \frac{\phi_i}{|\phi_i|} & \text{for } \phi_i \neq 0, \\ 0 & \text{else.} \end{cases} \quad (22)$$

We define the vector $\tilde{\phi} = \{\tilde{\phi}_i\}_{i=1}^N$, and then replace ϕ by $\tilde{\phi}$ when calculating q in Eq. (15). By the chain rule we have

$$\frac{\partial q}{\partial \phi_i} = \frac{\partial q}{\partial \tilde{\phi}_i} \frac{\partial \tilde{\phi}_i}{\partial \phi_i} = \frac{\partial q}{\partial \tilde{\phi}_i} \delta(\phi_i), \quad (23)$$

where δ denotes the delta Dirac function, i.e. $\delta(0) = 1$ and $\delta(\phi_i) = 0 \forall \phi_i \neq 0$.

In numerical implementations, it is desirable to replace $\tilde{\phi}_i$ by a smoothed approximation. The chosen approximation is

$$\tilde{\phi}_i \approx \frac{\phi_i}{\sqrt{\phi_i^2 + \epsilon}}, \quad (24)$$

where ϵ is a small positive number which has to be chosen. As ϕ_i is replaced by $\tilde{\phi}_i$, the gradient calculation in (18) and (19) also needs to be changed using (23). However, in [24] it was observed that good results were obtained if we just replace $\delta(\phi_i)$ in (23) by 1. That approach is also applied in this work. A numerical study of the improvement related to the speed of the modified algorithm, and a more thorough discussion of the advantages of this approach can be found in [24].

7.3 Updating the constants

By numerical experiments we have found it desirable to start with a rather large value of ϵ , and then decrease ϵ during the iterations. In this setting it is also natural to increase μ_p during the iterations. This differs from other related works [9, 20, 21], where a fixed μ_p has been used to reduce the ill-conditionness of the problem.

The minimization with respect to \mathbf{c} is a highly ill-conditioned process. It should therefore not be done too early or too frequently during the iterations. To further stabilize this process, we have applied a predefined search interval $[a_j, b_j]$ for each constant such that there will be no risk of producing values completely out of range.

7.4 Stopping rules

The applied method is searching a piecewise constant solution with a predefined number of constant values. For practical applications it may be desirable to stop the algorithm before the solution is strictly piecewise constant. The obvious advantage with this is that the change in the solution may be very small towards the end of the optimization, and therefore, stopping at an earlier stage will produce approximately the same solution within less time. In a real field, we do not know if there are sharp discontinuities between the regions,

and if this should be the case, these sharp discontinuities will probably not match the simulator grid perfectly.

We have found it difficult to find any suitable stopping criterion which will stop the iterations before the solution is strictly piecewise constant. In this work we will run the algorithm to a fixed number of iterations, or till both ϕ and \mathbf{c} have stopped changing.

8 Numerical results

In this section we will present some numerical examples where we study the performance of the presented method. The studied examples are synthetic cases where the true permeability field consists of two distinct permeability values. With two different permeability values, it is sufficient with one level set function to represent the field. The test reservoir is square and horizontal with constant thickness and no-flow outer boundaries. Except for the absolute permeability, the fluid and rock properties are held fixed through the simulations. In the field we have one injector positioned in the lower left corner, and one producer positioned in the upper right corner.

The relative permeability functions are defined by the Corey models;

$$\kappa_{rw} = \hat{\kappa}_{rw} \left(\frac{S_w - S_{wr}}{1 - S_{wr} - S_{or}} \right)^{e_w},$$

$$\kappa_{ro} = \hat{\kappa}_{ro} \left(\frac{S_o - S_{or}}{1 - S_{or} - S_{wr}} \right)^{e_o},$$

where the Corey exponents, e_w and e_o , the residual saturations, S_{wr} and S_{or} , and the endpoint permeabilities, $\hat{\kappa}_{rw}$ and $\hat{\kappa}_{ow}$, are assumed known. The numerical values for these properties are, together with the rest of the properties for the simulations, listed in Table 1.

The forward model [the solution of Eqs. (1)–(4) for a given function $q(\mathbf{x})$] is solved by applying an in-house reservoir simulator. In the simulator the equation error is minimized by applying Newton iterations, and the linear solver of choice is GMRES. The gradients, $\frac{\partial F}{\partial q}$, are obtained from the solution of the adjoint system of equations, see, e.g. [19].

For each reference permeability field we calculate the true values of saturation (S_w) and pressure (p_o) for the applied timesteps on the given grid. Thereafter synthetic measurements are constructed by adding noise to the calculated true values. The noise is assumed to be uncorrelated Gaussian noise with zero mean. In Table 2 the standard deviations which give the amount of added noise are listed. Notice that the uncertainties are larger for the seismic measurements than for the measurements in the wells. When calculating $J_{\text{tot}}(q)$ we use the correct uncertainties, according to the added noise, for constructing D_{well} and D_{seis} .

Table 1 Properties for the simulations

Reservoir dimensions	1,000 × 1,000 × 40 m	
Simulation grid	16 × 16 × 1 cells	
Porosity	0.2	
Viscosity	$\mu_w = 0.5 \times 10^{-3}$ Pa s	$\mu_o = 0.5 \times 10^{-3}$ Pa s
Endpoint relative permeabilities	$\hat{k}_{rw} = 0.1$	$\hat{k}_{ro} = 1$
Residual saturations	$S_{rw} = 0.2$	$S_{or} = 0.2$
Corey exponents	$e_w = 1.5$	$e_o = 2.5$
Initial saturation	$S_w = 0.2$	$S_o = 0.8$
Capillary pressure function	$P_c(S_w) \equiv 0$ kPa	
Injection rate	8% Of total pore volume per year ^a	
Production rate	Constant BHP = 200.0 bar	
Number of timesteps	192	
Total production time	3,000 days	
Number of seismic surveys	16 (i.e. approximately every 6 months)	

^a In Example 5 the injection rate is changed to 3.5% of total pore volume per year

Table 2 Standard deviations for the added noise

	Well data	Seismic data
Pressure	$\sigma_{p,\text{well}} = 1.0$ bar	$\sigma_{p,\text{seis}} = 2.5$ bar
Saturation	$\sigma_{S,\text{well}} = 0.025$	$\sigma_{S,\text{seis}} = 0.050$

The noise is larger for the seismic data than for the well data

The penalization parameter μ_p is increased slowly through the iterations. If k is the number of iterations, $\mu_p = 0.05 \times 1.01^k$ up till it reaches an upper bound (equal to 4) where we keep it fixed. Regarding the regularization parameter β , we have for each example first tried with a value of 5×10^{-3} . If this causes large oscillations in the solution, then the weight on the regularization is increased and a new optimization is preformed. The value of ϵ used to calculate $\tilde{\phi}$ is initially equal to 0.1, and is decreased by a factor of 0.98 until it reaches a lower bound equal to 10^{-7} . Both the Lagrangian parameter λ and the c_j values are updated each tenth iteration.

For each test case we start with $\phi^0 = 0$ in the entire domain except in the cells where we have wells. An initial $\phi^0 = 0$ means that we do not assume anything about the discontinuity. In the cells with a penetrating well, we assume that the approximate permeability value is known. The value of ϕ is therefore fixed equal to its correct value (-1 or 1 dependent of the initial \mathbf{c} value) in these cells.

For each of the constant values we define an interval $[a_j, b_j]$ within c_j should be estimated. The length of this interval will correspond to the *prior* uncertainty of the permeability value for the corresponding region. Because there are abilities for direct measurements of the permeability in the wells, we have applied a lower uncertainty for c_j in the regions where there is at least one well present, than for the regions with no wells. For the studied cases we have applied intervals $[a_j, b_j]$ with length equal 50% (no wells) and 30% (wells) of the difference between the two true values of q . The centre of the intervals are chosen equal to the true values. For example, if we assume the following; c_1 and c_2 are the true values, the region corresponding to c_1 has no wells present and there are one or more wells penetrating a region with permeability approximately equal to c_2 . Then the bounds will be

$$a_1 = c_1 - 0.25 \cdot |c_2 - c_1|, \quad b_1 = c_1 + 0.25 \cdot |c_2 - c_1|$$

and

$$a_2 = c_2 - 0.15 \cdot |c_2 - c_1|, \quad b_2 = c_2 + 0.15 \cdot |c_2 - c_1|.$$

In this work we start with initial c_j values on the lower and upper bound of the two intervals. We use the lower bound for the smallest c_j value and the upper bound for the highest c_j value, that is, if $c_1 < c_2$, then $c_1^0 = a_1$ and $c_2^0 = b_2$. Other approaches for choosing the initial values are also possible.

The algorithm is stopped after 1,000 iterations if ϕ^k and \mathbf{c}^k have not converged, in the sense of stopped changing, before this.

For each studied example we have plotted measures of the errors and the convergence. One of the measures is the equation error. We define $e_o(q, p_o, S_w)$ and $e_w(q, p_o, S_w)$ to be the equation residual for Eqs. (1) and (2), respectively, and let the equation error

$$E(q, p_o, S_w) = \sum_{i=0,w} \|e_i(q, p_o, S_w)\|_{L_2(\Omega \times [0,T])}. \quad (25)$$

Since Eqs. (1) and (2) are solved exactly in the forward model, the residual $E(q^k, m(q^k))$ should be zero or below a numerical error bound. To produce a measure of the amount of change in the solution in one iteration, we have calculated $E(q^k, m(q^{k-1}))$. Plotting corresponding equation errors versus iteration number can, even for linear equations (see [9]), produce highly oscillating curves. For non-linear equations the situation can be even worse. To easier detect the trend of these curves, we have also plotted a moving average of the $E(q^k, m(q^{k-1}))$. For the calculation of the moving average, we have used an average of the last 15 values of $E(q^k, m(q^{k-1}))$.

To measure the data fit we plot RMS values of J , J_{well} and J_{seis} versus the iteration number. The RMS value of a function J_α is defined as $\sqrt{2J_\alpha/n_\alpha}$, where n_α is the number of measurements included in J_α and $\alpha = \text{tot, well or seis}$.

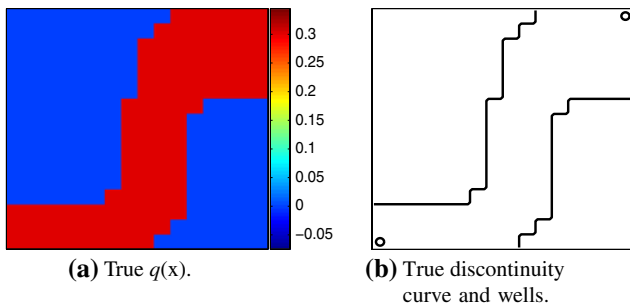


Fig. 3 Example 1: True permeability and the corresponding discontinuity. The constant levels are given by $\mathbf{c} = (0, 0.3)$, which corresponds to a permeability equal to 1 and 2 D. The *circles* in the corners are indicating the positioning of the wells

Other measures applied to check the convergence are $\|K(\phi^k)\|_{L_2}$ and $\|K(\tilde{\phi}^k)\|_{L_2}$. The difference between these two measures is that the first one indicates how fast ϕ^k reaches

the convergence values -1 and 1 , and the second one is a measure of how close \hat{q}^k is from being piecewise constant with only two levels.

Example 1 (S-shaped channel) In this example the true field is an S-shaped channel with high permeability from the injector till the producer. A plot of the field is shown in Fig. 3a, while the true discontinuity curve of the permeability is plotted in Fig. 3b. In this field there are three distinct piecewise constant regions, but since two of the regions have the same constant value, *one* level set function is sufficient to give a representation of it. This is related to the level set methods' nice feature of splitting and merging regions independent of their contours (see for example [28]).

In Fig. 4 the development of the estimates q^k and the signchange of ϕ^k are shown. Already after 50 iterations the estimate is quite close to the true field, but we need approximately 200 iterations to produce a field which is piecewise

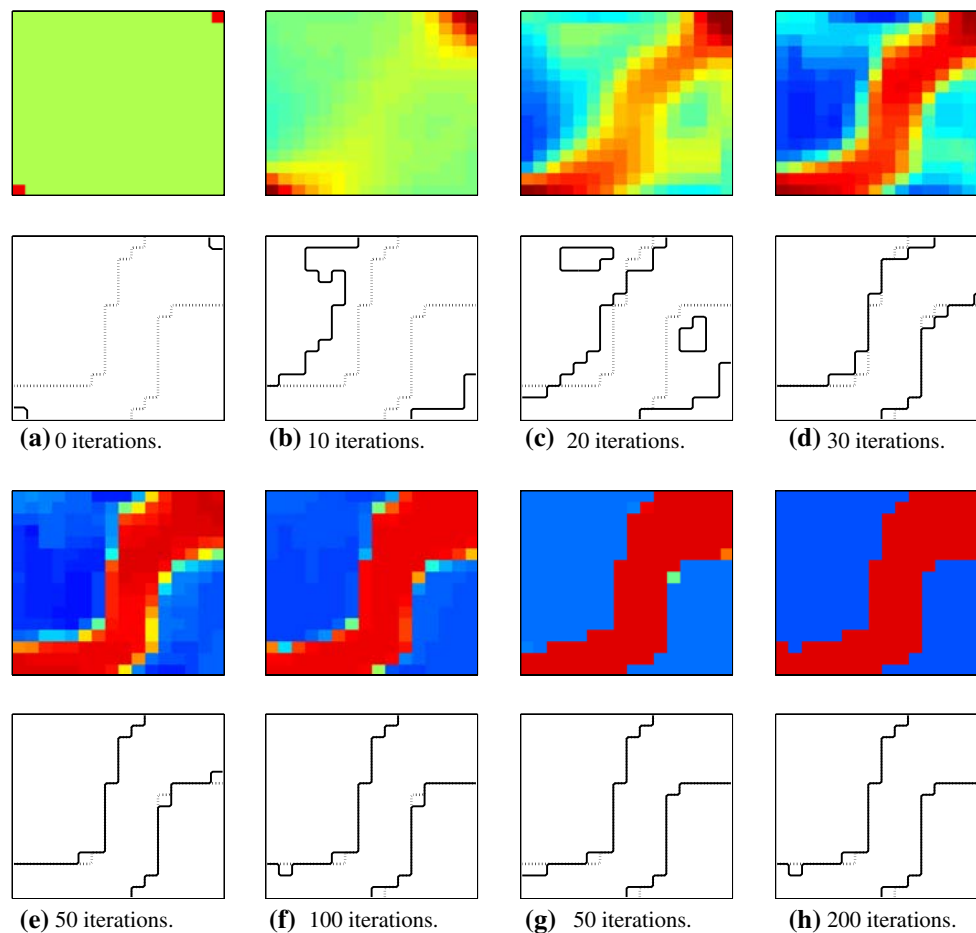


Fig. 4 Example 1: The estimated permeability for different iterations. In the upper rows q^k is plotted with the same colourmap as used in Fig. 3a. In the lower rows the signchanges of ϕ^k are shown by the *solid lines*, and the discontinuities of the true $q(\mathbf{x})$ are given by the *dotted lines*. Initially $\phi^0 = 0$ in the entire domain, except in the corners where the wells are located. In the intermediate iterations the values of ϕ^k will

evolve towards -1 or 1 in the different parts of the domain. After about 50 iterations the true field is approximately matched. We though need about 200 iterations before ϕ^k is (approximately) equal to 1 or -1 in all cells, and at this stage the field is piecewise constant with only two levels

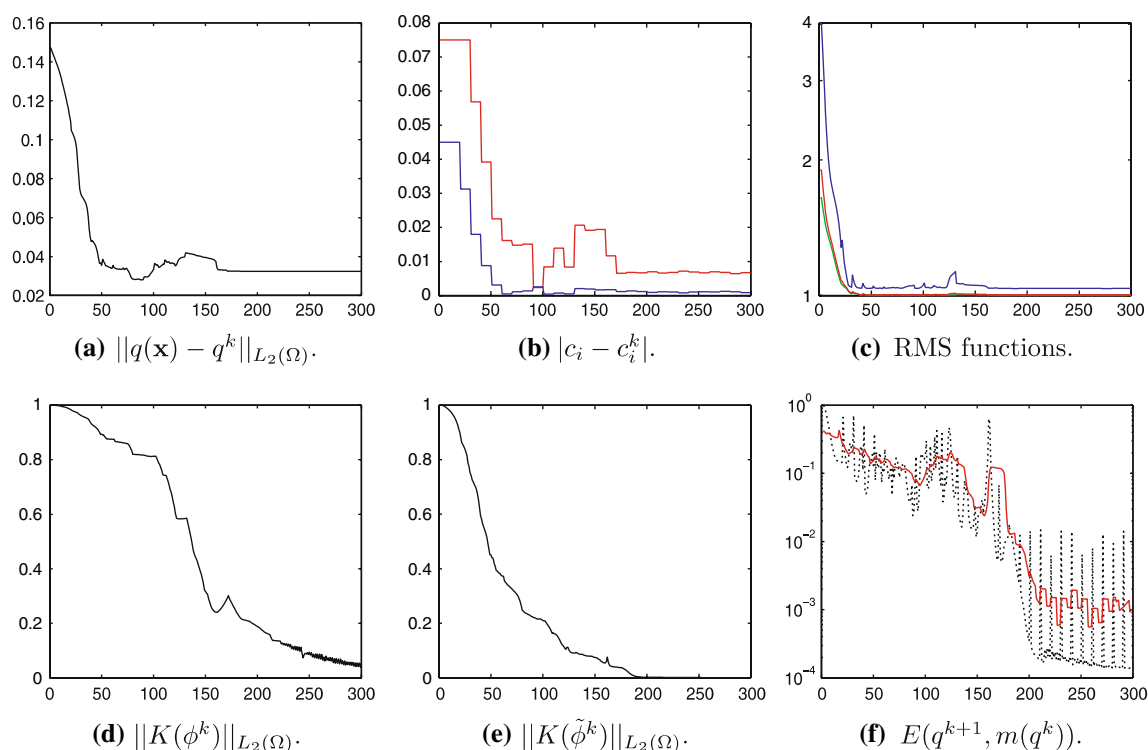


Fig. 5 Example 1: Error measures and convergence plots versus the iteration number. **a, b** Give the error in the computed q^k and c_i^k values. **c** The red curve gives the RMS values of J_{tot} , while the blue and the green curves are the RMS functions for J_{well} and J_{seis} , respectively. Measures

of the convergence of ϕ^k and $\tilde{\phi}^k$ are shown in **d** and **e**, respectively, while $E(q^{k+1}, m(q^k))$ in **f** is the norm of the equation residual. The red curve in **f** is an average of $E(q^{k+1}, m(q^k))$ for the last 15 iterations. The curves indicate convergence after about 200 iterations

constant with only two levels. From this time the solution stops changing.

Error measures and convergence curves are shown in Fig. 5. If we compare the different curves, we observe that the RMS functions (Fig. 5c) are decreasing much faster and for a shorter period than what is the case for all the other functions. After the initial rapid decrease, the RMS functions reach a stable value just above 1. The other measures are also reaching stable values, but after a higher number of iterations. Notice that the RMS functions are plotted in semilogarithmic scale, while most of the other functions (not the the equation residuals) are given in linear plots. This makes the difference in the behaviour of the curves even more clear.

The rapid decrease in the RMS functions can usually be explained by low sensitives with respect to the permeability changes in some areas of the field. The sought solution may therefore be difficult to find, and the convergence can be very slow towards the end of the optimization. The described phenomenon can be observed in all the tested examples and illustrates the ill-posedness of the treated inverse problem.

Example 2 (Horizontal barrier) In this example the true field is a horizontal barrier with low permeability across the entire

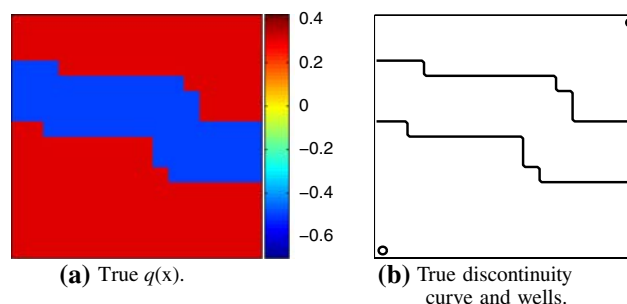


Fig. 6 Example 2: True permeability and the corresponding discontinuity. The constant levels are given by $c = (-0.5, 0.3)$, which corresponds to a permeability equal to 316 mD and 2 D. The circles in the corners are indicating the positioning of the wells

field. The inflow from the injector has to cross this barrier to reach the producer, see Fig. 6.

From the recovered q^* given in Fig. 7d we observe that the contour of the discontinuity is matching most of the main structures of the true field, but there are also some larger errors. Errors in the geometry of the discontinuities are typically related to errors also in the constant values (plotted in Fig. 8b). In this case the error in the c_j value corresponding to the low permeable region is not reduced significantly

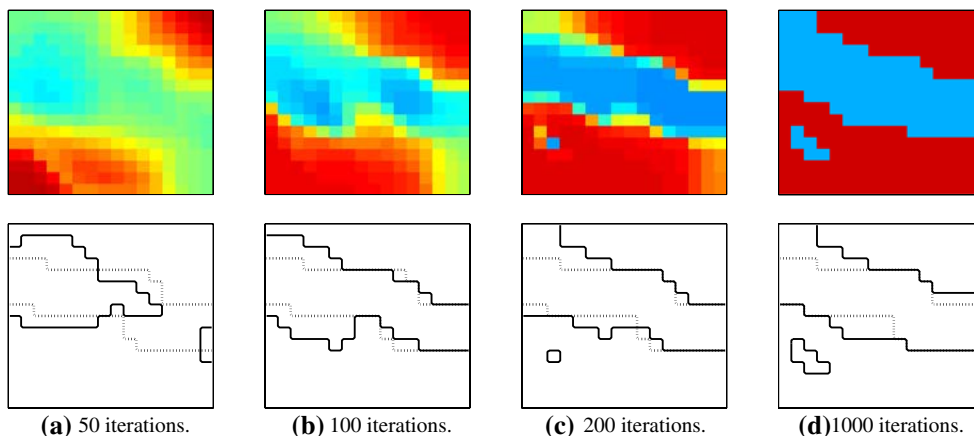


Fig. 7 Example 2: The estimated permeability for different iterations. In the upper figures q^k is plotted with the same colourmap as used in Fig. 6a. In the lower figures the signchanges of ϕ^k are shown by the *solid lines*, and the discontinuities of the true $q(x)$ are given by the *dotted lines*

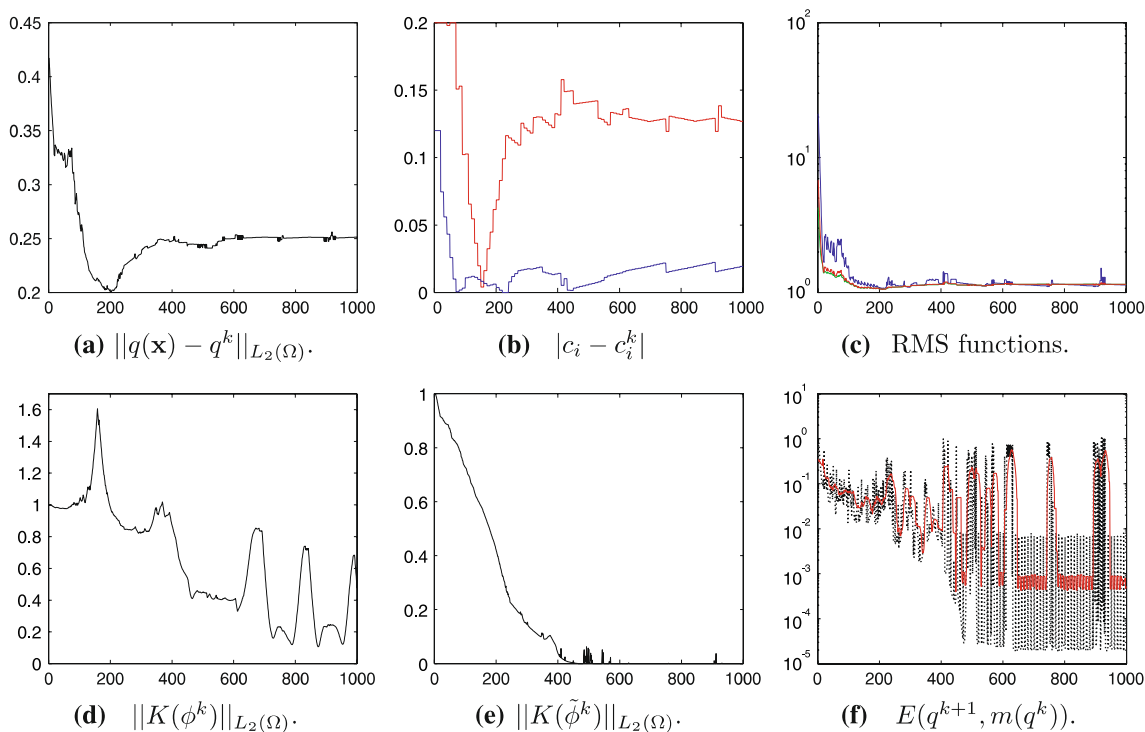


Fig. 8 Example 2: Error measures and convergence plots versus the iteration number. **a, b** Give the error in the computed q^k and c_i^k values. **c** The *red* curve gives the RMS values of J_{tot} , while the *blue* and the *green* curves are the RMS functions for J_{well} and J_{seis} , respectively. Measures

of the convergence of ϕ^k and $\tilde{\phi}^k$ are shown in **d** and **e**, respectively, while $E(q^{k+1}, m(q^k))$ in **f** is the norm of the equation residual. The *red* curve in **f** is an average of $E(q^{k+1}, m(q^k))$ for the last 15 iterations

from the initial value. We can also observe large oscillations in the equation residual (Fig. 8f), and that the constraint $\|K(\phi^k)\|_{L_2(\Omega)}$ (Fig. 8d) is not decreasing monotonically towards zero. This behaviour can sometimes occur when the method has large difficulties in finding a stable piecewise constant solution which reconcile the data.

Example 3 (Centered low permeable region) This example illustrates the recovery of a region with lower permeability in a region positioned in the middle of the field. The true field is shown in Fig. 9.

The solution plotted in Fig. 10 gives a field with lower permeability in approximately the correct region. The produced

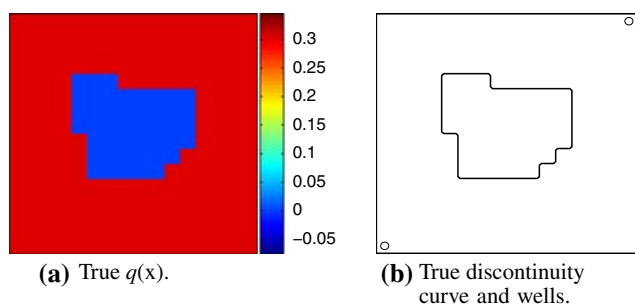


Fig. 9 Example 3: True permeability and the corresponding discontinuity. The constant levels are given by $\mathbf{c} = (0, 0.3)$, which corresponds to a permeability equal to 1 and 2 D. The circles in the corners are indicating the positioning of the wells

region with the lowest permeability is though not connected, and the shape is different the shape of the true solution. In spite of the error in the contour of the recovered region, the relative errors of the constant values c_j^k is low (Fig. 11 b).

For this example, we do not observe the same kind of oscillations or artifacts in the convergence plots (Fig. 11) as was the case for Example 2. The increase in $\|K(\phi^k)\|_{L_2(\Omega)}$ (Fig. 11e) in the early stages is because $|\phi^k|$ is getting much larger than 1 in some regions of the domain. This may happen when the Lagrangian multiplier, λ , is close to zero and the weight of the constraint, controlled by μ_p , is low. Later in the process, when these controlling terms get a higher weight, $\|K(\phi^k)\|_{L_2(\Omega)}$ starts to decrease towards zero as expected.

The error of q^k (Fig. 11a) has its lowest value at around 50 iterations. At this point the solution is not piecewise constant, but has smooth connections between the regions (Fig. 10a). The optimization method is only searching solutions which are piecewise constant with two regions. In this case the error

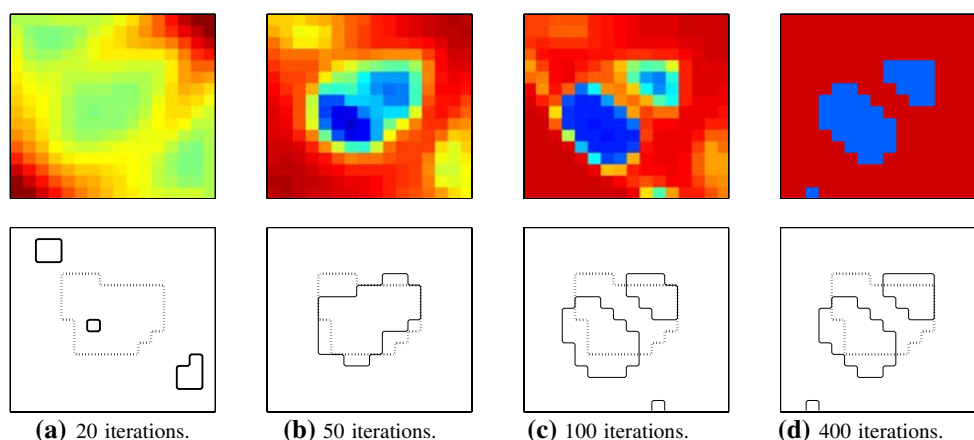


Fig. 10 Example 3: The estimated permeability for different iterations. In the upper figures q^k is plotted with the same colourmap as used in Fig. 9a. In the lower figures the signchanges of ϕ^k are shown by the solid

in the solution is increasing when the constraint $K(\phi) = 0$ is weighted higher and by this forcing the solution to be piecewise constant. Similar behaviour can also be observed in some of the other studied examples.

Example 4 (System of channels: low contrast) This example involves a more complicated field where two channels are crossing each other (see Fig. 12). The two channels are assumed to have the same permeability value, and together they produce a connected region with high permeability from the injector to the producer.

The estimates q^k and the sign of ϕ^k are shown for different iteration numbers in Fig. 13, and the convergence is shown in Fig. 14. Even with this complicated geometry, the level set method is able to recover the constant levels and the geometry of the discontinuities with a relatively low error. In the final solution, one of the branches of the channels is not connected to the rest of the system and the fine details of the discontinuity lines are not matched exactly. Though, the main structures of the field are recovered very well.

Example 5 (System of channels: high contrast) The true field, plotted in Fig. 15, is in this case equal to the field in Example 4 except that the constant values of the permeability in the two regions are changed. We have now a higher contrast between the two permeability values, and in addition, the lowest permeability value (equal to 32 mD) is here much lower than the corresponding permeability in the previous example (equal to 1 D). Because of the less permeable field, the constant injection rate per year is reduced to 3.5% of total pore volume for this example.

The results in Fig. 16 show that we are capturing a high permeable channel from the injector till the producer, but the other branches of the channels are not discovered. In some of the convergence plots in Fig. 17 we can observe large

lines, and the discontinuities of the true $q(\mathbf{x})$ are given by the dotted lines. A solution close to the true field is achieved after about 50 iterations, but this field is not fulfilling the piecewise constant requirement

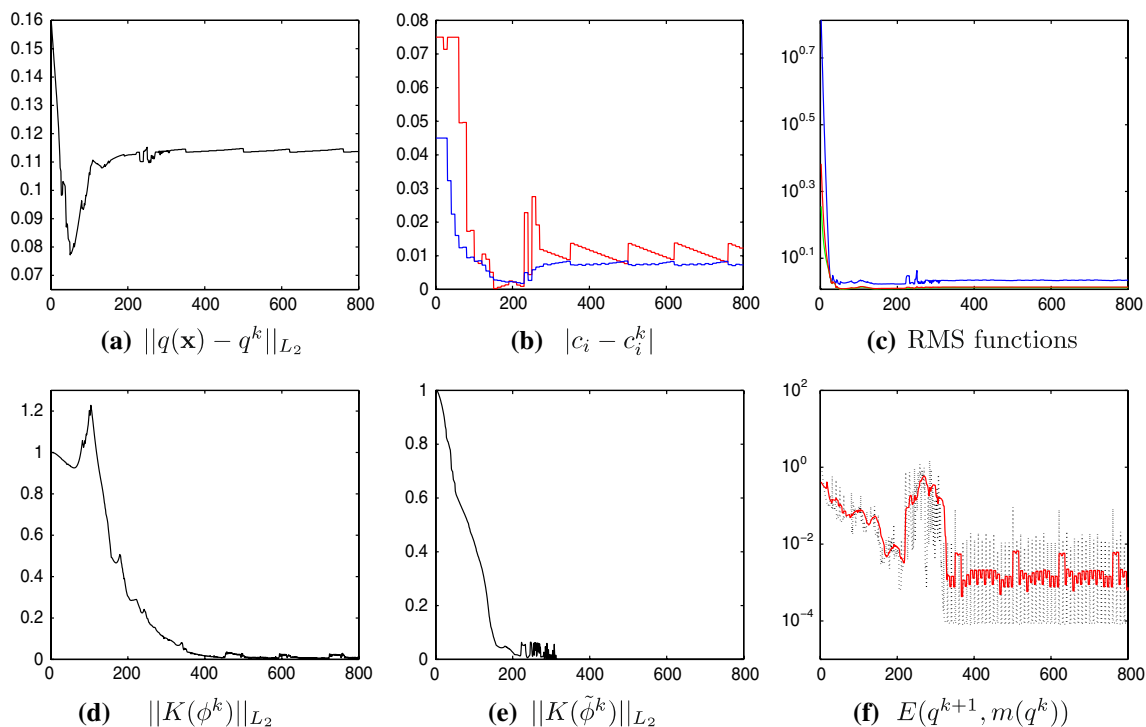


Fig. 11 Example 3: Error measures and convergence plots versus the iteration number. **a, b** Give the error in the computed q^k and c_j^k values. **c** The *red* curve gives the RMS values of J_{tot} , while the *blue* and the *green* curves are the RMS functions for J_{well} and J_{seis} , respectively. Measures

of the convergence of ϕ^k and $\tilde{\phi}^k$ are shown in **d** and **e**, respectively, while $E(q^{k+1}, m(q^k))$ in **f** is the norm of the equation residual. The *red* curve in **f** is an average of $E(q^{k+1}, m(q^k))$ for the last 15 iterations. The *curves* indicate convergence after about 400 iterations

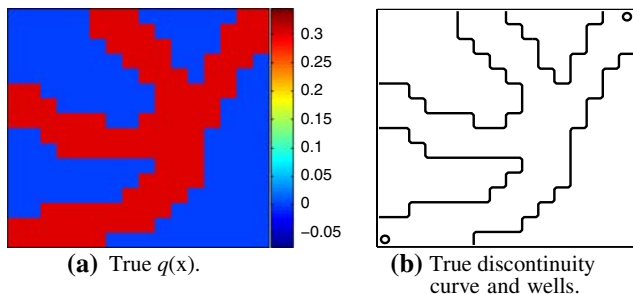


Fig. 12 Example 4: True permeability and the corresponding discontinuity. The constant levels are given by $\mathbf{c} = (0, 0.3)$, which corresponds to a permeability equal to 1 and 2 D. The *circles* in the corners are indicating the positioning of the wells

oscillations. This illustrates the difficulties of producing a piecewise constant field as a solution to this problem. The relative reduction in the error of q^k (Fig. 17a) is quite small for this example. This can be explained by the misclassification of some parts of the channels. The misclassified parts are by the method classified as low permeable regions, which in fact is less close to the true solution than the initial guess. The initial value, q^0 , is (except for the cells with wells) equal to the mean of c_1^0 and c_2^0 [given by $\phi = 0$ in Eq. (13)].

In Fig. 18 we have compared the simulated seismic data for the true fields used in Example 4 (low contrast) and Example 5 (high contrast). We have plotted p_o and S_w at the end of the simulations.

The plots of S_w show that for Example 4 the entire field will be flooded by water, while in Example 5, the main part of the flow will go in the high permeable region discovered by the level set method. In the last case, the flow will move very slowly in the low permeable regions and also in the parts of the channels which are not discovered by the optimization process. The comparison of the saturation fields shows that there is less information in the observation data from certain parts of the field in Example 5, than what is the case for Example 4. Due to this observation, it is natural that the field in Example 5 is the most difficult one to recover, and especially the regions with low flow may be problematic to reproduce.

From the comparison of the pressure data, it is more difficult to conclude anything about the amount of useful information in the data. It though seems like a constant gradient of the pressure field is preferable.

Returning to the convergence plots in Fig. 17, we observe that the errors in the recovered c_j values (Fig. 17 b) are rather small for this example. Normally large errors in the contours

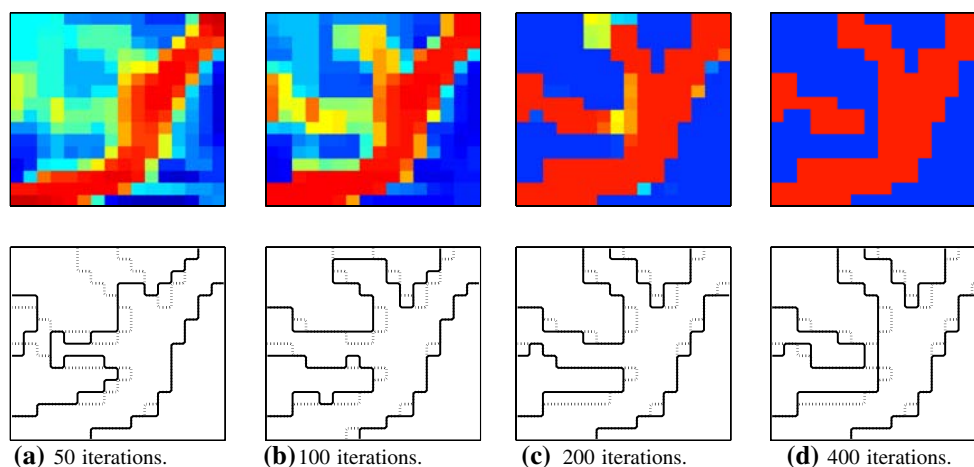


Fig. 13 Example 4: The estimated permeability for different iterations. In the upper figures q^k is plotted with the same colourmap as used in Fig. 12a. In the lower figures the signchanges of ϕ^k are shown by the *solid lines*, and the discontinuities of true $q(x)$ are given by the *dotted lines*

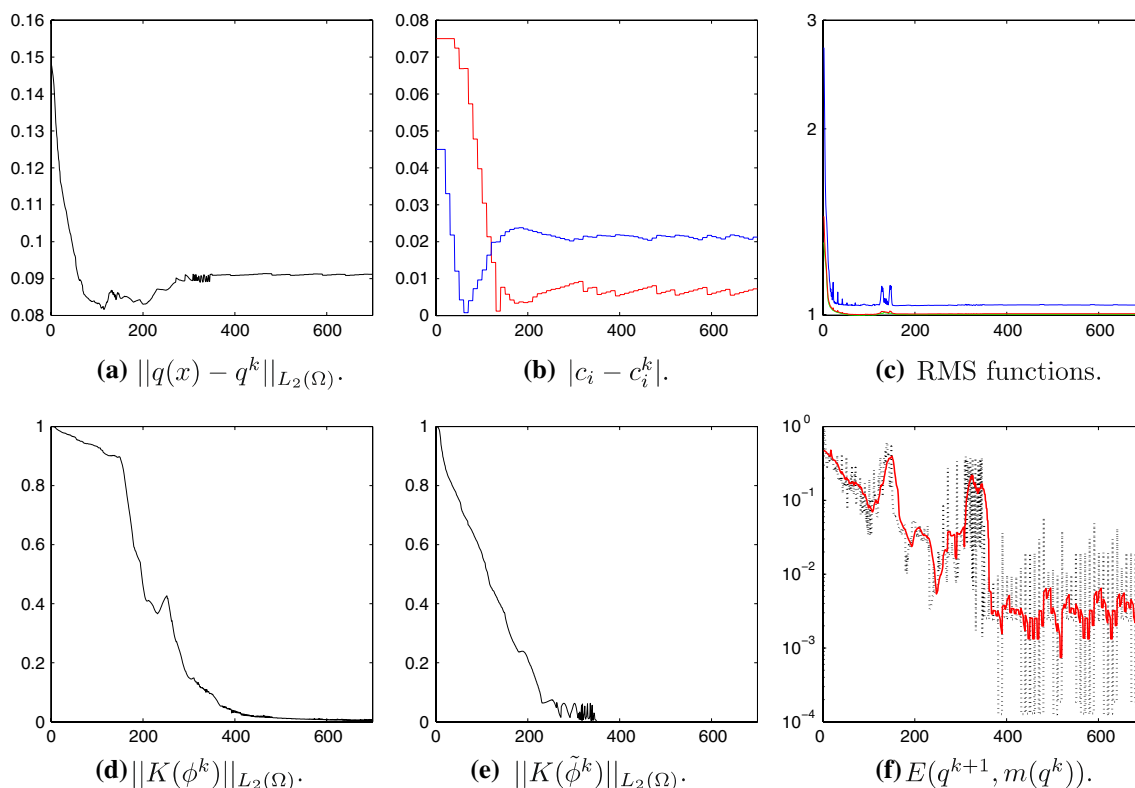


Fig. 14 Example 4: Error measures and convergence plots versus the iteration number. **a, b** Give the error in the computed q^k and c_i^k values. **c** The *red* curve gives the RMS values of J_{tot} , while the *blue* and the *green* curves are the RMS functions for J_{well} and J_{seis} , respectively. Measures

of the convergence of ϕ^k and $\tilde{\phi}^k$ are shown in **d** and **e**, respectively, while $E(q^{k+1}, m(q^k))$ in **f** is the norm of the equation residual. The *red* curve in **f** is an average of $E(q^{k+1}, m(q^k))$ for the last 15 iterations. The *curves* indicate convergence after about 400 iterations

will also force large errors in the c_j values (see Example 2). This is not the case for this example. The low errors of the recovered c_j values supports the conclusions from the analysis of the saturation fields, that the misclassified regions have

small impact on the behaviour of the flow in the reservoir, and will thereby give a low response in the data.

As stated in Sect. 2, we have for simplicity neglected the capillary pressure ($P_c = 0$) in our model. In a real case, P_c

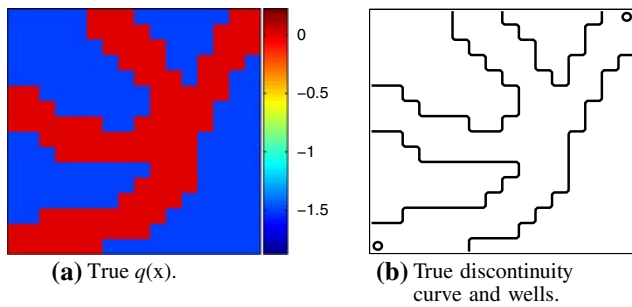


Fig. 15 Example 5: True permeability and the corresponding discontinuity. The constant levels are given by $\mathbf{c} = (-1.5, 0)$, which corresponds to a permeability equal to 32 mD and 1 D. The *circles* in the corners are indicating the positioning of the wells

will be a non zero continuous function depending on both the saturation and the spatial position \mathbf{x} . That is, over a discontinuity in the permeability field, there should be continuity in P_c , see [14]. It is reasonable to believe that a model with $P_c \neq 0$ may give more information about the jumps in the permeability, than our simplified model will do. In this way, a recovery of the studied fields may be easier without our simplifications related to the capillary pressure functions. Studies of the history matching problem with $P_c \neq 0$ is not looked into in this paper, but could be an issue for future works.

Example 6 (Inverse crime test) In this example, we try to address the concern of inverse crime. The true permeability field is exactly the same as in Example 4, shown in Fig. 12.

The observation data (well data and seismic data) are produced by running the commercial reservoir simulator “Eclipse” with the true permeability field, and then corrupted with Gaussian noise as described in Table 2. An in-house

reservoir simulator is employed to solve the inverse problem. The same grid and rock-fluid properties were used by both simulators. However, the fluids were assumed slightly compressible in Eclipse and incompressible in the in-house simulator. The forward model produced 192 time-steps, while 16 time-steps are selected out to act as the seismic data. To compare the results from Eclipse with our in-house simulator, we have run both simulators using the true permeability field, and then compared the seismic data by calculating the RMS errors for each of the 16 time-steps. The errors are shown in Fig. 19.

The estimates q^k and the sign of ϕ^k are shown for different iteration numbers in Fig. 20, and the convergence is shown in Fig. 21. In fact, because a lot of noise has been added to the observation data for all the numerical experiments, we believe that the inverse crime have been avoided. In this example, we even produce the observation data from a different simulator other than the simulator used in solving the inverse problem. From these figures, we see that the convergence is as good as in Example 4, which confirms that the method is stable with respect to an unknown model error.

9 Conclusions

We have applied a binary level set formulation for solving inverse two phase porous media flow problems. Both well data and seismic time-lapse data are utilized in the optimization process.

The method is searching a piecewise constant solution of the inverse problem, and it is regularized by a total variation norm. By the proposed approach we can produce a solution

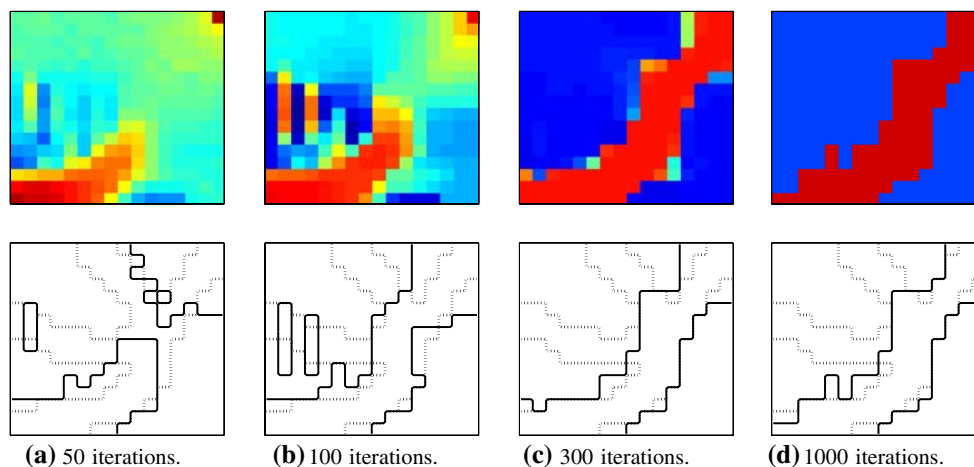


Fig. 16 Example 5: The estimated permeability for different iterations. In the upper figures q^k is plotted with the same colourmap as used in Fig. 15a. In the lower figures the signchanges of ϕ^k are shown by the

solid lines, and the discontinuities of the true $q(\mathbf{x})$ are given by the *dotted line*. Only the parts of the channels in the main flow direction is recovered

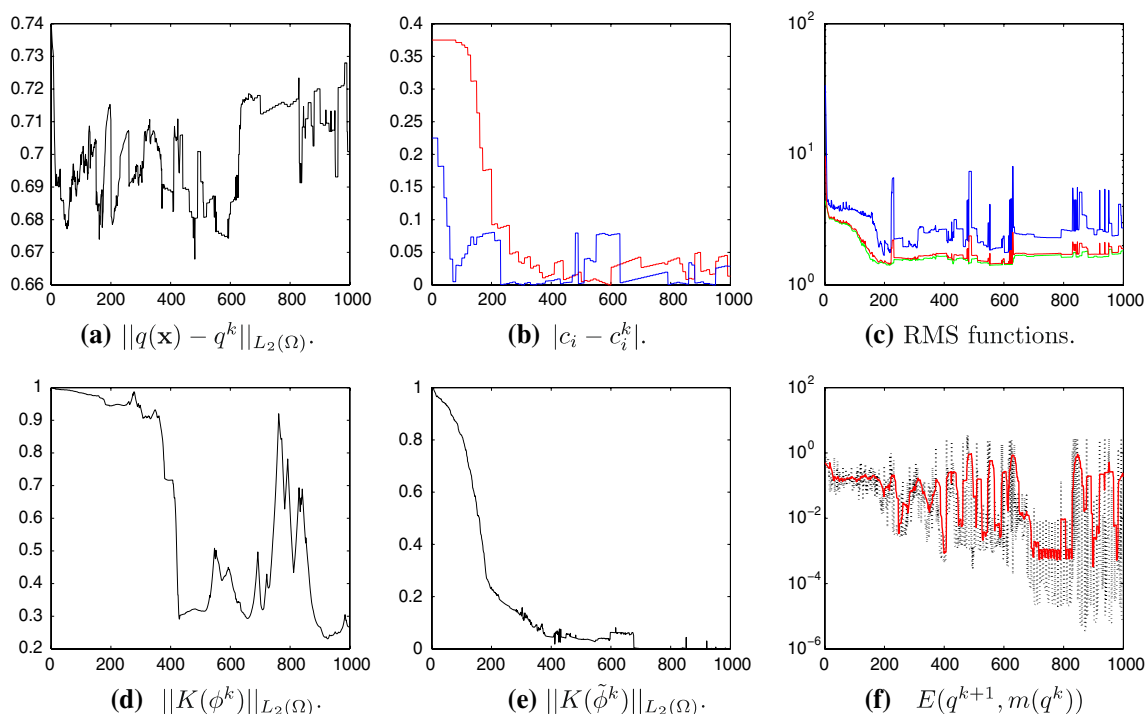


Fig. 17 Example 5: Error measures and convergence plots versus the iteration number. **a, b** Give the error in the computed q^k and c_i^k values. **c** The red curve gives the RMS values of J_{tot} , while the blue and the green curves are the RMS functions for J_{well} and J_{seis} , respectively. Measures

of the convergence of ϕ^k and $\tilde{\phi}^k$ are shown in **d** and **e**, respectively, while $E(q^{k+1}, m(q^k))$ in **f** is the norm of the equation residual. The red curve in **f** is an average of $E(q^{k+1}, m(q^k))$ for the last 15 iterations

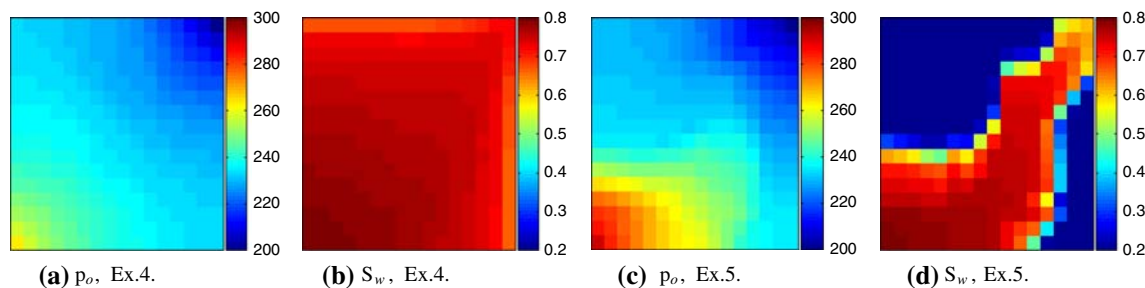


Fig. 18 Comparison of seismic data of the true field. Pressure and saturation are plotted at end of simulation (3,000 days). In Example 4, $\mathbf{c} = (0, 0.3)$ and the injection rate is equal to 8% of the total pore volume per year, while in Example 5, $\mathbf{c} = (-1.5, 0)$ and the injection rate

is equal to 3.5% of the total pore volume per year. In Example 4 the complete field is flooded by water at the end of the simulation, while in Example 5 only parts of it is flooded

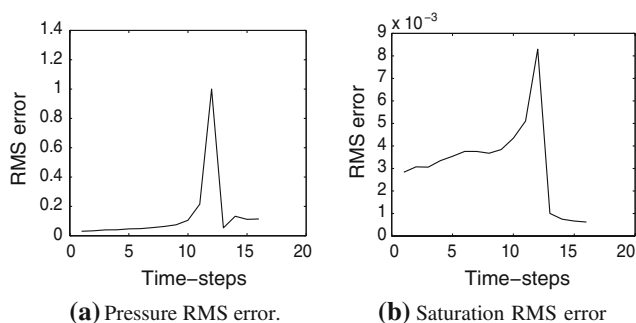


Fig. 19 Example 6: RMS error

with a predefined number of constant levels, and the geometries of the discontinuity curves are allowed to have arbitrary shapes only controlled by the total variation regularization. To produce the results we do not need any initial guess of the geometries of discontinuities, only a reasonable guess of the constant levels is required.

The numerical studies focus on piecewise constant permeability fields with two different constant levels. On most of the tested examples the method is able to recover the main structures of permeability fields with rather complicated geometries and with a moderate amount of noise

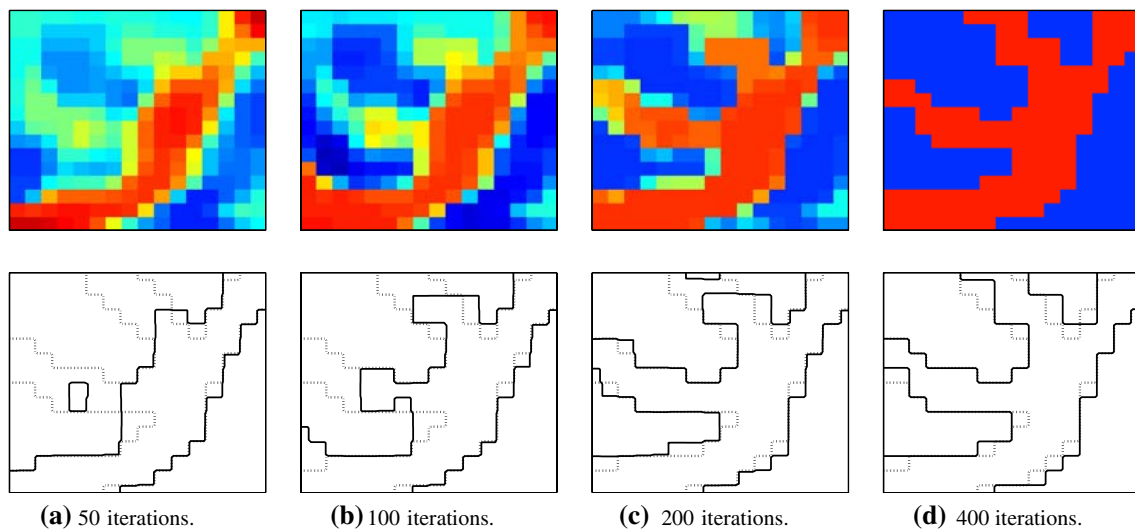


Fig. 20 Example 6: The estimated permeability for different iterations. In the upper figures q^k is plotted with the same colourmap as used in Fig. 12a. In the lower figures the signchanges of ϕ^k are shown by the *solid lines*, and the discontinuities of true $q(x)$ are given by the *dotted lines*

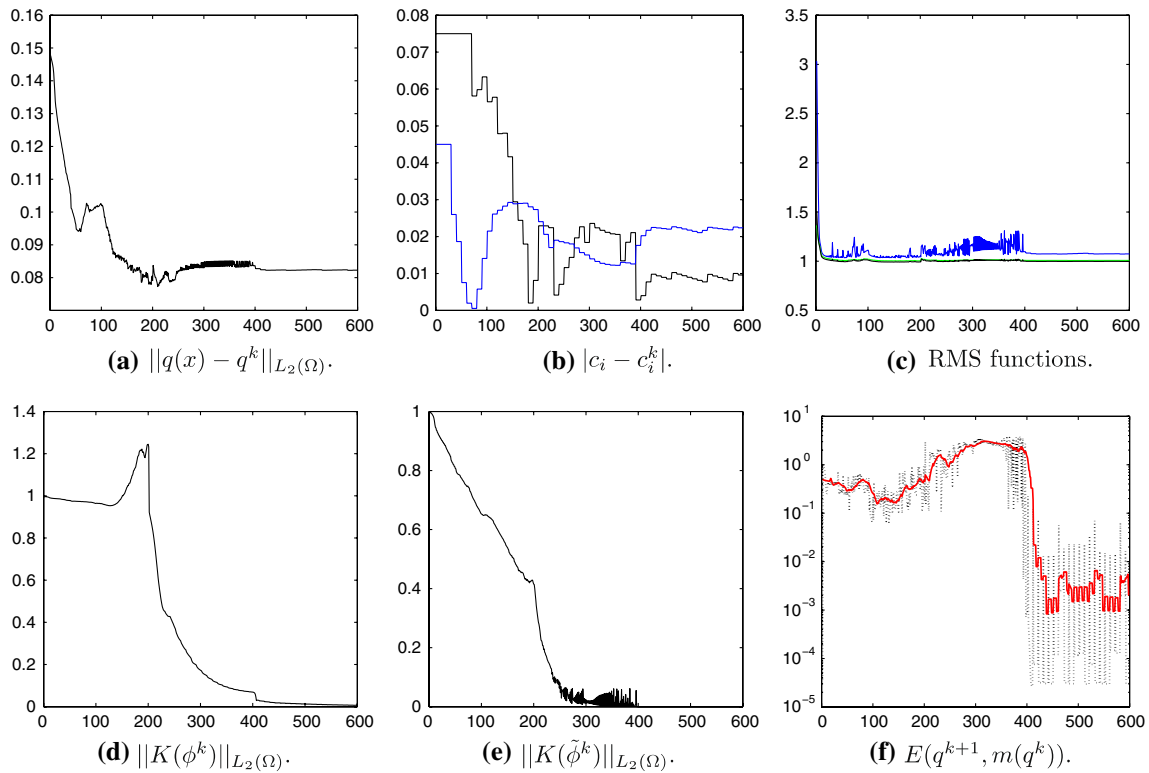


Fig. 21 Example 6: Error measures and convergence plots versus the iteration number. **a**, **b** Give the error in the computed q^k and c_i^k values. **c** The *red* curve gives the RMS values of J_{tot} , while the *blue* and the *green* curves are the RMS functions for J_{well} and J_{seis} , respectively. Measures

of the convergence of ϕ^k and $\tilde{\phi}^k$ are shown in **d** and **e**, respectively, while $E(q^{k+1}, m(q^k))$ in **f** is the norm of the equation residual. The *red* curve in **f** is an average of $E(q^{k+1}, m(q^k))$ for the last 15 iterations. The *curves* indicate convergence after about 400 iterations

added to the observation data. Misclassifications of regions seem to be due to less information from the data in certain parts of the domain.

Acknowledgments We gratefully acknowledge Daniel Christopher Doublet and Raymond Martinsen for providing their code for the forward reservoir simulator including gradient calculations, and for their help related to running this.

References

1. Aanonsen, S.I., Aavatsmark, I., Barkve, T., Cominelli, A., Gonard, R., Gosselin, O., Kolasinski, M., Reme, H.: Effect of scale dependent data correlations in an integrated history matching loop combining production data and 4D seismic data. In: Proceedings of the SPE reservoir simulation symposium, Houston, Texas, Feb 2003. SPE 79665
2. Aanonsen, S.I., Cominelli, A., Gosselin, O., Aavatsmark, I., Barkve, T.: Integration of 4D data in the history match loop by investigating scale dependent correlations in the acoustic impedance cube. In: Proceedings of the 8th European conference on the mathematics of oil recovery, Freiberg, Germany, 3–6 Sept 2002
3. Ascher, U.M., Haber, E.: Grid refinement and scaling for distributed parameter estimation problems. *Inverse Probl.* **17**, 571–590 (2001)
4. Ascher, U.M., Haber, E.: Computational methods for large distributed parameter estimation problems with possible discontinuities. In: Symp. inverse problems, design and optimization, 2004
5. Ascher, U.M., Haber, E., Huang, H.: On effective methods for implicit piecewise smooth surface recovery. *SIAM J. Sci. Comput.* **28**(1), 339–358 (2006)
6. Berre, I., Lien, M., Mannseth, T.: A level set corrector to an adaptive multiscale permeability prediction. *Comput. Geosci.* **11**(1), 27–42 (2007)
7. Burger, M.: A level set method for inverse problems. *Inverse Probl.* **17**, 1327–1355 (2001)
8. Burger, M., Osher, S.: A survey on level set methods for inverse problems and optimal design. UCLA, CAM-Report 04-02 (2004)
9. Chan, T., Tai, X.-C.: Level set and total variation regularization for elliptic inverse problems with discontinuous coefficients. *J. Comput. Phys.* **193**, 40–66 (2003)
10. Chavent, G., Liu, J.: Multiscale parameterization for the estimation of a diffusion coefficient in elliptic and parabolic problems. In: Proceedings of the 5th IFAC symposium on control of distributed parameter systems, Perpignan, France, June 1987
11. Chung, E., Chan, T., Tai, X.-C.: Electrical impedance tomography using level set representation and total variational regularization. *J. Comput. Phys.* **205**(1), 357–372 (2005)
12. Dorn, O., Miller, E., Rappaport, C.: A shape reconstruction method for electromagnetic tomography using adjoint fields and level sets. *Inverse Probl.* **16**:1119–1156 (2000). Special issue on Electromagnetic Imaging and Inversion of the Earth's Subsurface
13. Duijndam, A.J.W.: Bayesian estimation in seismic inversion. Part I: principles. *Geophys. Prospect.* **36**, 878–898 (1998)
14. Ersland, B.G., Espedal, M., Nybø, R.: Numerical methods for flow in a porous medium with internal boundaries. *Comput. Geosci.* **2**, 217–240 (1998)
15. Gibou, F., Fedkiw, R.: Fast hybrid k-means level set algorithm for segmentation. Stanford Technical Report (2002)
16. Gosselin, O., van den Berg, S., Cominelli, A.: Integrated history-matching of production and 4d seismic data. In: Proceedings of the 2001 SPE annual technical conference and exhibition, New Orleans, Louisiana, 30 Sept–3 Oct 2001. SPE 71599
17. Grimstad, A.-A., Mannseth, T., Nævdal, G., Urkedal, H.: Adaptive multiscale permeability estimation. *Comput. Geosci.* **7**(1), 1–25 (2003)
18. Ito, K., Kunisch, K., Li, Z.: Level-set function approach to an inverse interface problem. *Inverse Probl.* **17**, 1225–1242 (2001)
19. Li, R., Reynolds, A.C., Oliver, D.S.: History matching of three-phase flow production data. *SPE J.* **8**(4), 328–340 (2003)
20. Lie, J., Lysaker, M., Tai, X.-C.: A piecewise constant level set framework. *Int. J. Numer. Anal. Model.* **2**(4), 422–438 (2005)
21. Lie, J., Lysaker, M., Tai, X.-C.: A binary level set model and some applications to Mumford-Shah image segmentation. *IEEE Trans. Image Process.* **15**(5), 1171–1181 (2006)
22. Lien, M., Berre, I., Mannseth, T.: Combined adaptive multiscale and level-set parameter estimation. *Multiscale Model. Simul.* **4**(4), 1349–1372 (2005)
23. Liu, N., Oliver, D.S.: Automatic history matching of geologic facies. *SPE J.* **9**(4), 429–436 (2004)
24. Nielsen, L.K., Tai, X.-C., Aanonsen, S.I., Espedal, M.: A binary level set model for elliptic inverse problems with discontinuous coefficients. *Int. J. Numer. Anal. Modell.* **4**(1), 75–100 (2007)
25. Osher, S., Sethian, J.A.: Fronts propagating with curvature-dependent speed: algorithms based on hamilton-jacobi formulations. *J. Comput. Phys.* **79**(1), 12–49 (1988)
26. Santosa, F.: A level-set approach for inverse problems involving obstacles. *ESAIM Control Optim. Calc. Var.* **1**, 17–33 (1996)
27. Song, B., Chan, T.: A fast algorithm for level set based optimization. UCLA, CAM-Report 02-68 (2002)
28. Tai, X.-C., Chan, T.: A survey on multiple level set methods with applications for identifying piecewise constant functions. *Int. J. Numer. Anal. Model.* **1**(1), 25–47 (2004)
29. Tai, X.-C., Christiansen, O., Lin, P., Skjælaaen, I.: A remark on the mbo scheme and some piecewise constant level set methods. *Int. J. Comput. Vis.* **73**(1): 61–76 (2007). UCLA, CAM-Report 05-24
30. Tarantola, A.: *Inverse Problem Theory and Methods for Model Parameter Estimation*. SIAM, Philadelphia (2005)